

Exchange-bond structure and magnetization-step spectra of a diluted Heisenberg antiferromagnet on the square lattice: Lopsided two-exchange models

Yaacov Shapira*

Department of Physics and Astronomy, Tufts University, Medford, MA 02155

Valdir Bindilatti†

*Instituto de Física, Universidade de São Paulo,
Caixa Postal 66.318, 05315-970 São Paulo-SP, Brazil*

(Dated: October 24, 2018)

This paper on the theory of magnetization steps (MST's) from a strongly diluted antiferromagnet on the square lattice follows two others on the same topic. The preceding paper discussed Heisenberg models with two antiferromagnetic exchange constants of arbitrary magnitudes. The present paper specializes to “lopsided” models, in which the ratio of the two exchange constants is so small that the MST spectrum has certain characteristic features. One important feature is a gap which divides the MST spectrum into a low-field part and a high-field part. The models that are considered are the lopsided J_1 - J_2 model and the lopsided J_1 - J_3 model, where J_i is the exchange constant with the i th neighbor. The criteria that the ratios J_2/J_1 and J_3/J_1 must satisfy in order for these models to qualify as lopsided are obtained for magnetic ions with spin $S=5/2$. The bulk of the paper is devoted to a detailed exploration of the many connections between the exchange-bond structure of spin clusters and the MST spectra. These connections are established by extensive numerical simulations of spectra, supplemented by physical arguments. The concepts of “skeleton” and “decoration” are central to the discussion of the exchange-bond structure of cluster types with one or more J_1 bonds. A skeleton consists of the (strong) J_1 bonds and the spins attached to them. Other spins and exchange bonds, if there are any, are in the decoration. A skeleton is either “simple” or “compound.” A compound skeleton consists of several “fragments.” Simple skeletons and fragments are classified by types, which fully specify the J_1 bonds. Clusters containing simple skeletons and fragments of one type produce a “mono- skeleton” fine structure. It consists of groups of very close lines in the high-field part of the spectrum. Spectral lines in the low-field part of the spectrum are related to the weak exchange bonds. Some of these lines arise from pure- J_2 (or pure- J_3) cluster types. Others are related to J_2 (or J_3) bonds in decorations of mixed clusters. The connections between these low-field lines and the exchange-bond structure of the decorations are discussed in detail. Two alternative methods of measuring the weak exchange constant are outlined. One involves low-field lines from J_2 (or J_3) pairs. The other involves some high-intensity lines in the high-field fine structure. The contribution of clusters of sizes $n_c > 5$ to the magnetization is approximated by the corrective quintets (CQUIN's) method. A detailed description of this method is given in an Appendix.

PACS numbers: 05.50.+q, 75.50.Ee, 71.70.Gm, 75.10.Jm, 75.10.Nr, 75.60.Ej

I. INTRODUCTION

This is the third theoretical paper on magnetization steps (MST's) from a strongly diluted Heisenberg antiferromagnet on the square lattice. The first paper¹ (also called I) was based on the nearest-neighbor (NN) cluster model, or J_1 model. The second paper² (also called II) discussed “generic” and “specific” cluster models with two antiferromagnetic (AF) exchange constants. The generic $J^{(1)}$ - $J^{(2)}$ model placed no restriction on the ratio $J^{(2)}/J^{(1)}$ between the second-largest and largest exchange constants. Similarly, there was no restriction on the ratio of the exchange constants in the two specific models that were considered: 1) the J_1 - J_2 and the J_1 - J_3 models, where J_i is the exchange constant with the i th neighbor.

Numerical simulations of the magnetization curve, M versus B , and of the derivative curve, dM/dB versus B , were also carried out in II. The pattern of the peaks in

the derivative curve was defined as the “MST spectrum.” For the J_1 - J_2 model the simulated spectra indicated that when the ratio J_2/J_1 is “very small” the spectrum has the following features:

1. The spectrum consists of a low-field part and a high-field part. The two parts are separated by a “gap” in which there are no discernable spectral lines.
2. The magnetization curve exhibits a plateau in the field region of the gap. This plateau corresponds to the apparent saturation in the J_1 model.¹
3. In the high-field part of the spectrum, each spectral line that exists in the J_1 model may, and usually does, develop a fine structure (FS).
4. Separations of spectral lines in this FS are of order $\Delta b_2 \sim 1$, where b_2 is the secondary reduced magnetic field, defined by Eq. (3b) of II. The corresponding separations ΔB are of order $|J_2|/g\mu_B$, where g is the g-factor and μ_B is the Bohr magneton.

5. Typical line separations Δb_2 in the low-field part of the spectrum are also of order 1.

When the ratio J_2/J_1 in the J_1 - J_2 model is sufficiently small that the spectrum has the five features listed above, the model is called “lopsided.” The lopsided J_1 - J_3 model is defined in a similar manner. The relevant small ratio is then J_3/J_1 , and line separations ΔB in the high-field FS, and in low-fields, are controlled by J_3 .

The present paper is devoted to the lopsided J_1 - J_2 and J_1 - J_3 models. Among the topics that will be discussed are:

1. The numerical criteria that the ratios J_2/J_1 and J_3/J_1 must satisfy in order for J_1 - J_2 and J_1 - J_3 models to qualify as lopsided;
2. The concepts of “skeleton” and “decoration,” for the exchange-bond structure of clusters;
3. Connections between many features of the MST spectra and the relevant skeletons and decorations;
4. Features of the spectrum that are most useful for measuring the second-largest exchange constant.

As in I and II, the present paper includes extensive numerical simulations of MST spectra. The simulations are only for magnetic ions with spin $S=5/2$, and only for zero temperature, $T=0$. Some simulations at finite T are included in the following paper as a part of the data analysis.³

In calculations of the spectra (dM/dB vs B) the infinite sum in Eq. (2) of II is truncated at the maximum cluster size $n_{\max}=5$, and the remainder is ignored. In simulations of the magnetization M , on the other hand, the remainder is approximated by the corrective quintets (CQUIN’s) method. This method is described in Appendix A.

II. REQUIREMENTS FOR A MODEL TO QUALIFY AS LOPSIDED

A. The various criteria

In order for a $J^{(1)}$ - $J^{(2)}$ cluster model to qualify as “lopsided,” the ratio $J^{(2)}/J^{(1)}$ must satisfy two numerical criteria: a “general criterion” and a “gap criterion.” The general criterion is

$$J^{(2)}/J^{(1)} < 1/10. \quad (1)$$

That is, the two exchange constants must differ by at least one order of magnitude. The “gap criterion” requires the ratio $J^{(2)}/J^{(1)}$ to be sufficiently small that a gap, with no spectral lines, separates the low-field and high-field parts of the spectrum.

In contrast to the general criterion, the gap criterion depends on S , on the maximum cluster size n_{\max} at which the sum in Eq. (2) of II is truncated, and, in principle, also on the specific cluster model. These dependencies

cause the gap criterion to be more complicated than the general criterion. Both the general criterion and the gap criterion must be satisfied. The more stringent of the two criteria is the “governing criterion” that a model is lopsided.

B. Gap criterion for $S=5/2$ and $2 \leq n_{\max} \leq 5$

The criteria for the existence of a gap in the J_1 - J_2 and J_1 - J_3 models were obtained only for $S=5/2$ and only for $2 \leq n_{\max} \leq 5$. It turned out that at least for these values of S and n_{\max} , the numerical criterion that the ratio J_3/J_1 must satisfy in order for the J_1 - J_3 model to be lopsided is the same as the criterion for the ratio J_2/J_1 in the J_1 - J_2 model. Therefore, only the ratio J_2/J_1 in the J_1 - J_2 model will be discussed in detail.

The first step was to obtain a necessary condition that the ratio J_2/J_1 must fulfill in order for a gap to exist. This condition depends on n_{\max} . Numerical simulations then showed that for $n_{\max}=2$ and 3 the necessary condition is also sufficient, so that it is the gap criterion. For $n_{\max}=4$ and 5, however, the necessary condition is not quite sufficient. A minor adjustment was therefore required to obtain the gap criterion.

1. Necessary condition for a gap

Cluster types that give rise to MST’s in the J_1 - J_2 model belong to three categories: pure- J_1 , pure- J_2 , and “mixed.” Only the last category involves both J ’s. The gap is in the total spectrum, from all cluster types of all categories. The necessary condition for a gap was obtained by considering only the spectrum from the pure cluster types, i.e., mixed cluster types were excluded.

The pure- J_2 cluster types produce spectral lines only in the low-field part of the spectrum. On the other hand, the pure- J_1 cluster types produce lines in the high-field part of the spectrum. A necessary condition for a gap is that the highest B for any MST from the pure- J_2 cluster types is below the lowest B for any MST from the pure- J_1 cluster types. The pure- J_2 cluster types are all the cluster types of the (parent) J_2 model. The pure- J_1 cluster types are a known subset of the cluster types of the (parent) J_1 model. The two parent models are isomorphic (see Appendix A of II). For any choice of n_{\max} , only lines from cluster types with sizes $n_c \leq n_{\max}$ are considered.

For $S=5/2$, the primary reduced fields b_1 at the MST’s from each cluster type of the J_1 model are given in Table II of Ref. 1. The secondary reduced fields b_2 at the MST’s from the isomorphic cluster types in the J_2 model are the same. For cluster sizes not exceeding $n_{\max}=2, 3, 4$, and 5, the highest value of b_2 is $b_{2,\max}=10, 15, 20$, and 25, respectively. The lowest b_1 is $b_{1,\min}=2$ when $n_{\max}=2$ or 3, and 0.950 when $n_{\max}=4$ or 5.

Expressing $b_{2,\max}$ and $b_{1,\min}$ in terms of B , the necessary condition for a gap is $J_2/J_1 < (b_{1,\min}/b_{2,\max})$.

Thus, the necessary condition for $n_{\max}=2, 3, 4, 5$ is $J_2/J_1 < 0.200, 0.133, 0.0475, 0.0380$, respectively.

2. The gap criterion

The sufficient condition for a gap was obtained from numerical simulations that also included the mixed cluster types. For $n_{\max}=2$ and 3, the necessary condition was found to be sufficient. Therefore, the gap criterion for $n_{\max}=2$ is $J_2/J_1 < 0.200$. For $n_{\max}=3$, the gap criterion is $J_2/J_1 < 0.133$.

When n_{\max} is either 4 or 5, the sufficient condition for a gap is slightly more stringent than the necessary condition. The reason is that among the lines in the high-field part of the spectrum, the line with the lowest b_1 is from a mixed cluster, not from a pure- J_1 cluster. The relevant mixed-cluster type is 4-3 (4-1 in the J_1 - J_3 model). Including the lowest b_1 from this cluster type, the gap criterion for $n_{\max}=4$ is $J_2/J_1 < 0.0450$. For $n_{\max}=5$, the gap criterion is $J_2/J_1 < 0.0364$.

C. Governing criterion for a lopsided model when $S=5/2$ and $2 \leq n_{\max} \leq 5$

The more stringent of the general criterion and the gap criterion is the governing criterion. For $n_{\max}=2$ and 3 the governing criterion is the general criterion, $J_2/J_1 < 0.10$. For $n_{\max}=4$ and 5, on the other hand, the gap criterion is the governing criterion. The governing criterion is therefore $J_2/J_1 < 0.0450$ for $n_{\max}=4$, and $J_2/J_1 < 0.0364$ for $n_{\max}=5$.

D. Selecting n_{\max}

The selection of n_{\max} in the calculation of the spectrum depends on several considerations. One is that n_{\max} cannot exceed the largest size of clusters whose Hamiltonians can be diagonalized with available resources. Sometimes, however, n_{\max} is chosen to be lower than the upper limit of technical capabilities, because the labor of calculating the spectrum is reduced substantially.

Because spectral lines from cluster types with sizes $n_c > n_{\max}$ are lost in the simulation, a choice of a lower n_{\max} implies a greater loss of spectral lines. However, this greater loss is not always significant. If the concentration x of the magnetic ions is sufficiently low, only a negligible fraction of the total number of magnetic ions are in clusters with $n_c > n_{\max}$. In the present paper, all the calculated spectra are based on the choice $n_{\max}=5$.

III. SKELETONS AND DECORATIONS

A. Introductory remarks

The MST spectrum can always be obtained numerically using the procedures described in Ref. 2. Quite often, however, the numerically-obtained spectrum does not immediately reveal some of the underlying physics. A major goal of the present paper is to expose the connections between many features of the MST spectrum and the exchange-bond structures of the relevant clusters. The discussion below is mainly for the lopsided J_1 - J_2 model. The physics of the lopsided J_1 - J_3 model is very similar.

Three categories of cluster types give rise to MST's in the J_1 - J_2 model: pure- J_2 cluster types, pure- J_1 cluster types, and mixed cluster types. The spectra from the pure cluster types have already been discussed in Sec. II B. Therefore, the mixed cluster types are the main (but not the only) focus of the remaining discussion in this paper. The majority of all spectral lines are, in fact, from mixed cluster types.

The concepts of “skeleton” and “decoration” are central to the discussion of the exchange-bond structure of mixed cluster types. They are not essential concepts for pure- J_1 cluster types. However, the use of these concepts both for mixed and for pure- J_1 cluster types has the advantage of a more uniform presentation. The common feature of mixed and pure- J_1 clusters is that each such cluster contains at least one J_1 bond. In the physical picture that will be adopted here, any cluster with at least one J_1 bond consists of a skeleton and a decoration.

B. Skeletons

The following definitions and properties for the lopsided J_1 - J_2 model also apply to the lopsided J_1 - J_3 model. All that is necessary is to replace “ J_2 ” by “ J_3 .”

1. Definition of a skeleton

Consider a cluster with at least one J_1 bond. The skeleton of this cluster consists of all the J_1 bonds in the cluster together with all the spins that are attached to these J_1 bonds. The much weaker J_2 bonds, if any are present, are never included in a skeleton. Some spins in the skeleton (called “skeleton-spins”) may be attached to J_2 bonds. But even in such cases the J_2 bonds are not included in the skeleton.

The cluster types of the J_1 - J_2 model were shown in Figs. 1 and 2 of the preceding paper.² Figures 1 and 2 of the present paper are revised versions of the same figures. The revisions emphasize the skeletons. Skeleton-spins are represented by solid circles, in contrast to other spins which are shown as empty circles. The J_1 bonds (always included in the skeleton) are represented by solid








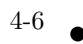



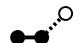

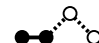




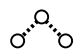
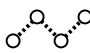
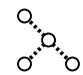
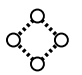
Skeleton type	Cluster Size, n_c			
	1	2	3	4
(4A) _S				4-1  4-2  4-3 
(4B) _S				4-4 
(4C) _S				4-5 
(3) _S			3-1  3-2 	4-6  4-7  4-8 
(2) _S		2-1 	3-3 	4-9  4-10  4-11 
(2) _S -(2) _S				4-12 
	1-1 	2-2 	3-4 	4-13  4-14  4-15 

FIG. 1: Cluster types of the lopsided J_1 - J_2 model, up to size $n_c=4$. This figure is similar to Fig. 1 of Ref. 2, except that it emphasizes the skeletons. Skeleton-spins are shown as solid circles, whereas other spins are represented by empty circles. The solid lines represent J_1 bonds. The J_2 bonds are shown as dotted lines. The first column gives the skeleton type for all the skeletons in the same row.

lines, whereas the J_2 bonds (never considered as parts of the skeleton) are shown as dotted lines.

The cluster types of the J_1 - J_3 model were shown earlier in Figs. 3 and 4 of Ref. 2. Revised versions of these figures, which emphasize the skeletons, are shown in Figs. 3 and 4 of the present paper. The format is similar to that in Figs. 1 and 2, except that dotted lines represent J_3 bonds.

2. Simple and compound skeletons

Skeletons are either “simple” or “compound.” A skeleton is simple if and only if all the skeleton-spins are connected to each other by a continuous path (or paths) of J_1 bonds. For a compound skeleton there are at least two skeleton-spins which are not connected by a continuous path of J_1 bonds. Because these two spins are still in the same cluster, they must be connected by at least one continuous path of exchange bonds, but such a path must include at least one J_2 bond. Examples of compound skeletons are cluster type 4-12 in Fig. 1, and cluster types 5-36 up to 5-41 in Fig. 2.

A compound skeleton always consists of two or more “fragments.” All spins in the same fragment are connected by a continuous path (or paths) of J_1 bonds. Any continuous exchange path between spins in different fragments must include at least one J_2 bond.

All cluster types in Figs. 1–4 contain no more than 5 spins. Each fragment must contain at least two spins. Therefore, any compound skeleton in these figures has

two fragments, with 2 or 3 spins in each fragment.

3. Skeleton types

Consider simple skeletons first. By itself, any simple skeleton is identical to some realization of one of the cluster types of the J_1 model. This cluster type of the J_1 model is chosen as the type of the simple skeleton. The label for the skeleton type is also the same as the label for the cluster type in the J_1 model (as defined in Ref. 1), except that it is surrounded by a parenthesis and is followed by a subscript “S.” For example, a simple skeleton which is identical to a NN pair in the J_1 model is a skeleton of type (2)_S. In the J_1 model the cluster type gives the complete set of J_1 bonds in the cluster. Similarly, the type of a simple-skeleton gives the complete set of J_1 bonds in the simple skeleton.

Compound skeletons also are classified by types. As a first step, each fragment is assigned a “fragment type.” The procedure is similar to the assignment of a type to a simple skeleton. The fragment type gives the complete set of J_1 bonds in the fragment. For the compound skeleton as a whole, the skeleton type is given by the sequence of the fragment types. The order in the sequence is arbitrary. For example, the compound skeletons of quintet types 5-36, 5-37, and 5-38 in Fig. 2 are all composed of two fragments: a NN pair and a NN triplet. These are cluster types 2 and 3 of the J_1 model (see Fig. 3 of Ref. 1). The compound skeletons of the three mentioned cluster types in Fig. 2 are therefore of type (2)_S-(3)_S or,

Skeleton type	Cluster Size $n_c = 5$
(5A) _S	5-1 5-2 5-3 5-4 5-5 5-6
(5B) _S	5-7 5-8 5-9
(5C) _S	5-10
(5D) _S	5-11
(4A) _S	5-12 5-13 5-14 5-15 5-16 5-17
(4B) _S	5-18 5-19
(4C) _S	5-20
(3) _S	5-21 5-22 5-23 5-24 5-25 5-26 5-27 5-28 5-29
(2) _S	5-30 5-31 5-32 5-33 5-34 5-35
(3) _S -(2) _S	5-36 5-37 5-38
(2) _S -(2) _S	5-39 5-40 5-41
	5-42 5-43 5-44 5-45

FIG. 2: The quintet types of the lopsided J_1 - J_2 model. This figure is similar to Fig. 2 of Ref. 2 except that the skeletons are emphasized. The first column gives the skeleton type.

alternatively, $(3)_S$ -(2)_S.

Figures 1–4 are arranged so that cluster types with the same skeleton type appear in the same row. The skeleton type is given in the left column. The cluster types in the bottom row of each of these figures have no J_1 bonds. Therefore, they have no skeletons.

C. Decorations

1. Decorations of mixed clusters

Any mixed cluster has both a skeleton and a decoration. The decoration consists of all the exchange bonds

that are not in the skeleton, together with all the spins that are not in the skeleton, if there are any such spins. For a mixed J_1 - J_2 cluster type the decoration includes all the J_2 bonds, and all the spins that are not attached to any J_1 bond. Each decoration-spin must be attached to at least one J_2 bond; otherwise it would have been a single, and not a spin in a mixed J_1 - J_2 cluster. In Figs. 1–4 the decoration spins are among the spins that are represented by empty circles.

Decorations of mixed J_1 - J_2 cluster types may be divided into two classes:

1. “Spinless decorations” (also called pure-bond decorations) contain no spins. They consist only of J_2 bonds. All the spins of the cluster are then in










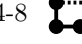
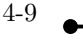



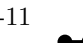
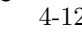


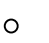
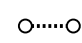


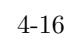

Skeleton type	Cluster Size, n_c			
	1	2	3	4
(4A) _S				4-1  4-2  4-3 
(4B) _S				4-4 
(4C) _S				4-5 
(3) _S			3-1  3-2 	4-6  4-7  4-8  4-9 
(2) _S		2-1 	3-3 	4-10  4-11  4-12 
(2) _S -(2) _S				4-13  4-14 
	1-1 	2-2 	3-4 	4-15  4-16  4-17 

FIG. 3: Cluster types of the lopsided J_1 - J_3 model, up to size $n_c=4$. The skeletons are emphasized by using solid circles for skeleton-spins and solid lines for J_1 bonds. Dotted lines represent J_3 bonds. The skeleton type is given in the first column.

the skeleton. Therefore, all the J_2 bonds are between skeleton-spins. Examples of spinless decorations are those of cluster types 3-2, 4-2, 4-3, 4-4, and 4-5 in Fig. 1, and of types 5-2 up to 5-11 in Fig. 2.

2. A “spinned decoration” (also called a spin-bond decoration) contains at least one spin. Any spin in such a decoration must be attached to at least one J_2 bond, but it cannot be attached to a J_1 bond (otherwise, it would have been a skeleton-spin). Examples of spinned decorations are those in cluster types 3-3, and 4-6 up to 4-11 in Fig. 1, and in cluster types from 5-12 up to 5-35 in Fig. 2.

Although all J_2 bonds of a mixed cluster are always parts of the decoration, there is no requirement that all J_2 bonds of a mixed cluster must be between decoration-spins. Some J_2 bonds can be between skeleton-spins, as in cluster types 4-7 and 4-8 (Fig. 1).

Analogous definitions of spinless and spinned decorations apply to mixed clusters of the lopsided J_1 - J_3 model. Their properties too are analogous to those of spinless and spinned decorations of the lopsided J_1 - J_2 model.

2. Null decorations of pure- J_1 clusters

The concept of a “decoration” will also be used in connection with pure- J_1 clusters. This usage may seem strange because all spins and all exchange bonds of a pure- J_1 cluster are already included in its skeleton, i.e., the skeleton is the entire cluster. One may therefore

reasonably say that a pure- J_1 cluster has no decoration. The use of decorations in connection with pure- J_1 cluster types is just a matter of convenience.

The “existence” of a decoration for a pure- J_1 cluster is merely a formality. A “null decoration” is defined as a decoration that contains no spins and no exchange bonds. All pure- J_1 clusters then have null decorations. Obviously, having a null decoration is equivalent to having no decoration.

In summary, there are three categories of decorations: Spinless (pure-bond)) and spinned (spin-bond) decorations occur in mixed clusters. Null decorations occur in pure- J_1 clusters.

D. Sizes of skeletons, decorations, and fragments

The size of a skeleton is the number of spins in the skeleton, labeled as n_S . The size n_D of a decoration is the number of spins in the decoration. For null decorations and spinless decorations, $n_D=0$. The size n_c of any cluster type c composed of a skeleton and a decoration is

$$n_c = n_S + n_D. \quad (2)$$

The size n_F of a fragment of a compound skeleton is the number of spins in the fragment. The size of the compound skeleton is the sum of n_F over all fragments in the skeleton,

$$n_S = \sum n_F. \quad (3)$$





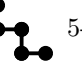
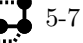
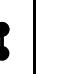
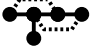





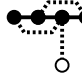


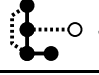

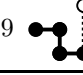

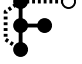






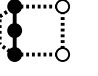
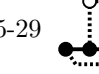

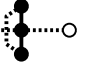
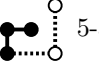
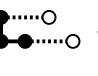

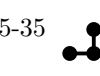
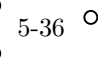
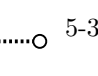
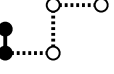
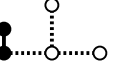
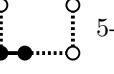
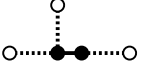
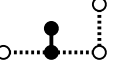
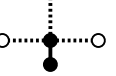
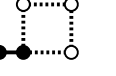

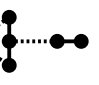
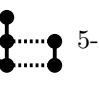

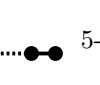

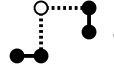
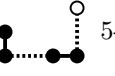
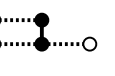
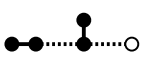
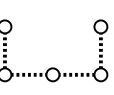
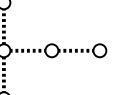
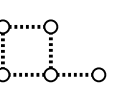
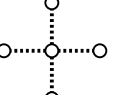
Skeleton type	Cluster Size $n_c = 5$
(5A) _S	5-1  5-2  5-3  5-4  5-5  5-6  5-7 
(5B) _S	5-8  5-9  5-10 
(5C) _S	5-11 
(5D) _S	5-12 
(4A) _S	5-13  5-14  5-15  5-16  5-17  5-18  5-19  5-20 
(4B) _S	5-21  5-22  5-23 
(4C) _S	5-24 
(3) _S	5-25  5-26  5-27  5-28  5-29  5-30  5-31  5-32  5-33  5-34  5-35  5-36  5-37 
(2) _S	5-38  5-39  5-40  5-41  5-42  5-43  5-44 
(3) _S -(2) _S	5-45  5-46  5-47  5-48  5-49  5-50 
(2) _S -(2) _S	5-51  5-52  5-53  5-54 
	5-55  5-56  5-57  5-58 

FIG. 4: The quintet types of the lopsided J_1 - J_3 model. The skeletons are emphasized. The skeleton type is given in the first column.

IV. MONO-SKELETON AND POLY-SKELETON FINE STRUCTURES IN THE HIGH-FIELD PART OF THE SPECTRUM

The concepts of skeletons and skeleton types bring insight into the physics of the FS in the high-field part of the spectrum. The major cause of this FS is illustrated by the following example.

A. Example of a mono-skeleton FS

Several cluster types of the J_1 - J_2 model have a simple skeleton of type (2)_s. The lower part of Fig. 5 shows simulated spectra from all these cluster types. The spectra are plotted against the primary reduced field b_1 . The parameters for these simulations are: $J_2/J_1=0.028$, $S=5/2$, $n_{\max}=5$, and $T=0$. For these parameters the high-field part of the spectrum starts at $b_1=0.920$. The lower part of Fig. 5 shows that in this high-field part, spectral lines from all the cluster types with a (2)_s simple skeleton are very close to $b_1=2, 4, \dots, 10$.

The upper part of Fig. 5 shows the spectra from all cluster types with a compound skeleton containing a fragment of type (2)_s. All these cluster types also produce spectral lines very near to $b_1=2, 4, \dots, 10$. Several of these cluster types (types 5-36, 5-37, and 5-38) also produce additional lines near $b_1=7, 9, \dots, 15$. These three cluster types have a compound skeleton of type (3)_s-(2)_s.

In the (parent) J_1 model, the spectral lines of cluster type 2 (NN pair) are exactly at $b_1=2, 4, \dots, 10$. In the same model, cluster type 3 (NN triplet) produces lines exactly at $b_1=7, 9, \dots, 15$. The obvious interpretation of the high-field results in Fig. 5 is, therefore, that all cluster types of the J_1 - J_2 model that contain a simple skeleton or a fragment of type (2)_s produce high-field lines at nearly the same magnetic fields as those of lines produced by cluster type 2 in the J_1 model. The additional high-field lines in the upper part of Fig. 5, from cluster types 5-36, 5-37, and 5-38, are due to the (3)_s fragment in the (3)_s-(2)_s compound skeleton. The magnetic fields at these additional lines are nearly the same as those of the lines from the triplets (cluster type 3) of the J_1 model.

The total MST spectrum is a statistically-weighted superposition of spectra from all cluster types of the model. There are 18 cluster types with a (2)_s skeleton/fragment. Together, they produce groups of very close lines near $b_1=2, 4, \dots, 10$. Line separations Δb_2 within each group are of order 1. The very close lines in each group may be viewed as a FS splitting of a single line from NN pairs (cluster type 2) in the J_1 model. This FS, will be called the (2)_s “mono-skeleton” FS. The dark lines in Fig. 5 represent the spectral lines of this mono-skeleton FS.

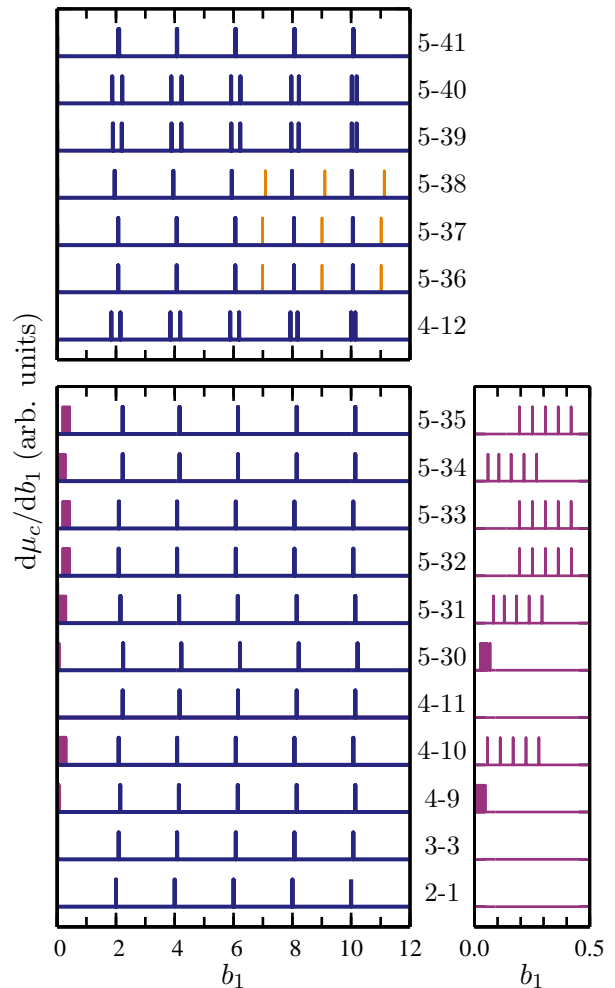


FIG. 5: The spectra of all cluster types that contribute to the (2)_s mono-skeleton FS in the J_1 - J_2 model. Lines in the (2)_s mono-skeleton FS are darker (dark blue). The lower part of the figure shows the spectra from all cluster types with a simple skeleton of type (2)_s. The panel to the right of the lower part gives an expanded view of the low-field spectra. The upper part of the figure shows the spectra from all cluster types with a compound skeleton containing a fragment of type (2)_s. The labels for the cluster types follow Figs. 1 and 2. The abscissa is the primary reduced magnetic field b_1 . All line intensities are chosen to be equal.

B. Other mono-skeleton FS's in the J_1 - J_2 model

The results below are based on simulations of spectra from various cluster types of the J_1 - J_2 model. Once again the parameters are: $J_2/J_1=0.028$, $S=5/2$, $n_{\max}=5$, and $T=0$. The discussion focuses on mono-skeleton FS's. All such FS's are in the high-field part of the spectrum.

The bottom part of Fig. 6 shows the spectra from all cluster types with a simple skeleton of type (3)_s. All the high-field lines are very near $b_1=7, 9, \dots, 15$. The upper part of Fig. 6 shows the spectra from the three cluster types that contain a (3)_s fragment. The same three cluster types already appeared in Fig. 5. They

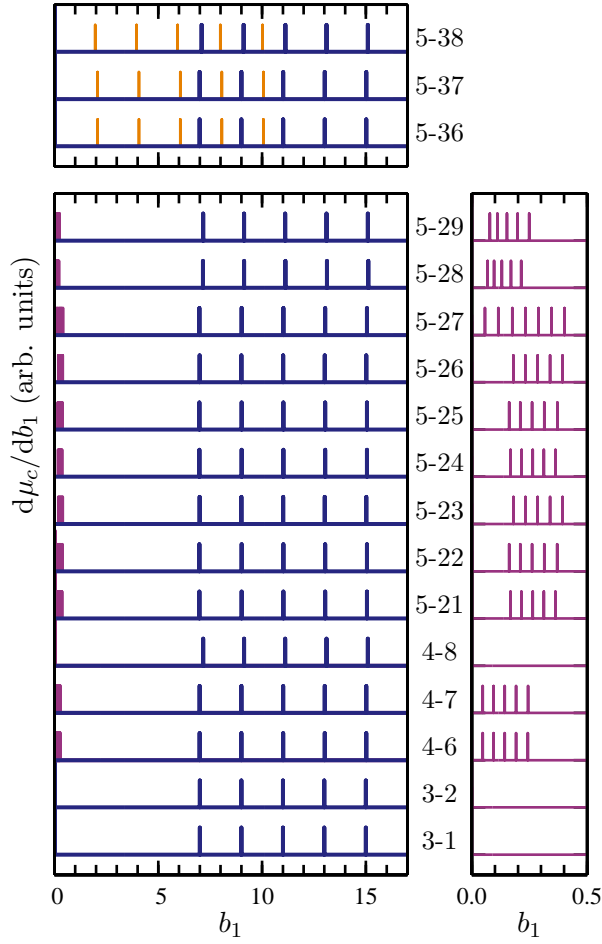


FIG. 6: The spectra of all cluster types that contribute to the $(3)_S$ mono-skeleton FS in the J_1 - J_2 model. The format is similar to that in Fig. 5, except that the darker (dark blue) lines are now the lines in the $(3)_S$ mono-skeleton FS. The labels for the cluster types follow Figs. 1 and 2.

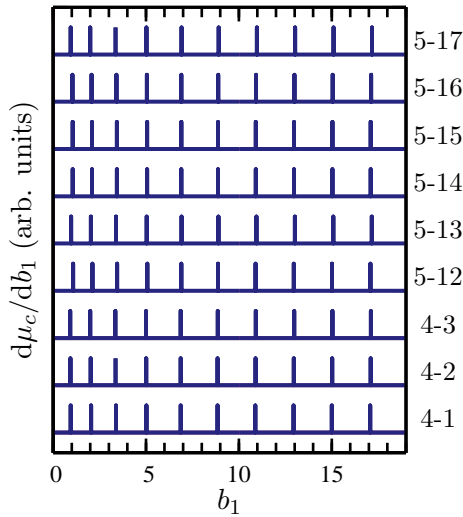


FIG. 7: The $(4A)_S$ mono-skeleton spectra of the J_1 - J_2 model. The labels for the cluster types follow Figs. 1 and 2.

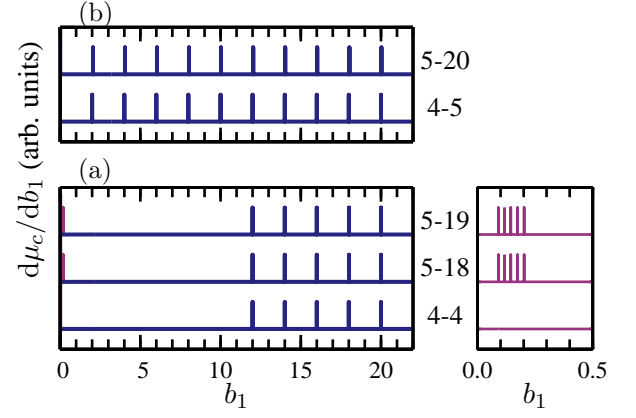


FIG. 8: (a) The spectra of all cluster types that contribute to the $(4B)_S$ mono-skeleton FS in the J_1 - J_2 model. Only the darker (dark blue) lines are in the $(4B)_S$ mono-skeleton FS. The panel on the right gives an expanded view of the low-field spectra. (b) The $(4C)_S$ mono-skeleton spectra of the J_1 - J_2 model.

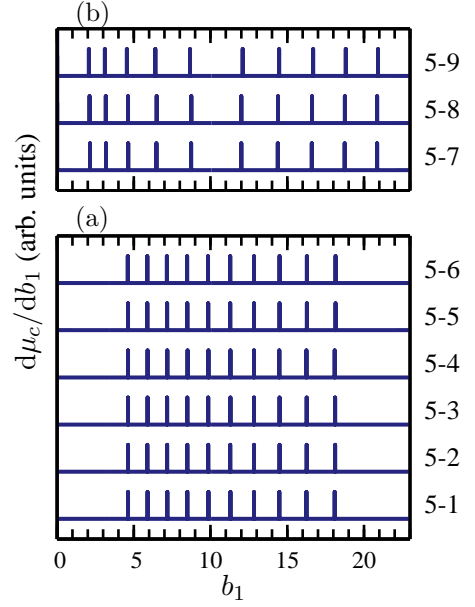


FIG. 9: (a) The $(5A)_S$ mono-skeleton spectra of the J_1 - J_2 model. (b) The $(5B)_S$ mono-skeleton spectra of the J_1 - J_2 model.

contain both a $(3)_S$ fragment and a $(2)_S$ fragment. The $(3)_S$ fragment produces lines very near $b_1=7, 9, \dots, 15$, and the $(2)_S$ fragment produces lines very close to close to $b_1=2, 4, \dots, 10$.

The $(3)_S$ mono-skeleton FS is produced by the 17 cluster types with $(3)_S$ skeletons/fragments. This FS consists of groups of very close lines near $b_1=7, 9, \dots, 15$. Line separations, Δb_2 , in each group are of order 1. Each group of very close lines may be viewed as a FS splitting of one of the triplet lines (cluster type 3) in the J_1 model. In Fig. 6, the $(3)_S$ mono-skeleton FS is represented by dark lines.

All cluster types in Figs. 1 and 2 have sizes $n_c \leq 5$. The only possible fragment types are $(2)_S$ and $(3)_S$. The spectra from all cluster types containing such fragments have already been included in Figs. 5 and 6. The only high-field lines that are not included in Figs. 5 and 6 are from cluster types with simple skeletons of sizes $n_S=4$ or 5.

Figure 7 shows the spectra from all cluster types with a $(4A)_S$ skeleton. In the parent J_1 model the $4A$ quartets produce lines at $b_1=0.950, 2.041, 3.389, \dots$ (see Table II of Ref. 1). The combined spectrum from all nine cluster types in Fig. 7 consists of groups of several very close lines near each of these values of b_1 . This is the $(4A)_S$ mono-skeleton FS of the lopsided J_1 - J_2 model.

Figure 8(a) shows the spectra from the three cluster types with a $(4B)_S$ skeleton. The high-field lines from these cluster types are all very close to each other. The $(4B)_S$ mono-skeleton FS consists only of these high-field lines (shown darker). The two cluster types in Fig. 8(b) are responsible for the $(4C)_S$ mono-skeleton FS.

Figure 9(a) shows the spectral lines from the six cluster types in Fig. 2 that have a $(5A)_S$ skeleton. The $(5A)_S$ mono-skeleton FS includes all these lines. The $(5B)_S$ mono-skeleton FS is produced by the three cluster types in Fig. 9(b).

There is only one cluster type with a $(5C)_S$ skeleton. Its spectrum (not shown) is very similar to that of cluster type $5C$ in the (parent) J_1 model. All the lines are in the high-field part of the spectrum. Because there is only one cluster type, a mono-skeleton FS does not develop. Similar remarks apply to the one cluster type with a $(5D)_S$ skeleton.

C. Poly-skeleton FS in the high-field part of the spectrum

A poly-skeleton FS occurs whenever different mono-skeleton FS's, associated with different skeleton/fragment types, overlap in the same region of the magnetic field. For example, Table I of Ref. 1 shows that in the parent J_1 model all five lines from cluster type 2 (at $b_1=2, 4, \dots, 10$) coincide with the first five lines from cluster type $4C$. In the lopsided J_1 - J_2 model, each group of very close lines in the $(2)_S$ mono-skeleton FS will overlap a group of very close lines in the $(4C)_S$ mono-skeleton FS.

In the example just given, spectral lines in the J_1 model from two different cluster types of that model were at exactly the same fields. Exact coincidence of lines from different cluster types of the J_1 model, however, is not the only possible origin of a poly-skeleton FS. A close proximity of lines from different cluster types of the J_1 model is another possibility. For example, in the J_1 model cluster type $4A$ has a line at $b_1=2.041$. This line is quite close to the line at $b_1=2$ from cluster type 2. Unless J_2/J_1 is extremely small, the $(2)_S$ and $(4A)_S$ mono-skeleton FS's, by themselves, will generate a poly-skeleton FS near $b_1=2$. However, as already noted, cluster type $4C$ of the J_1

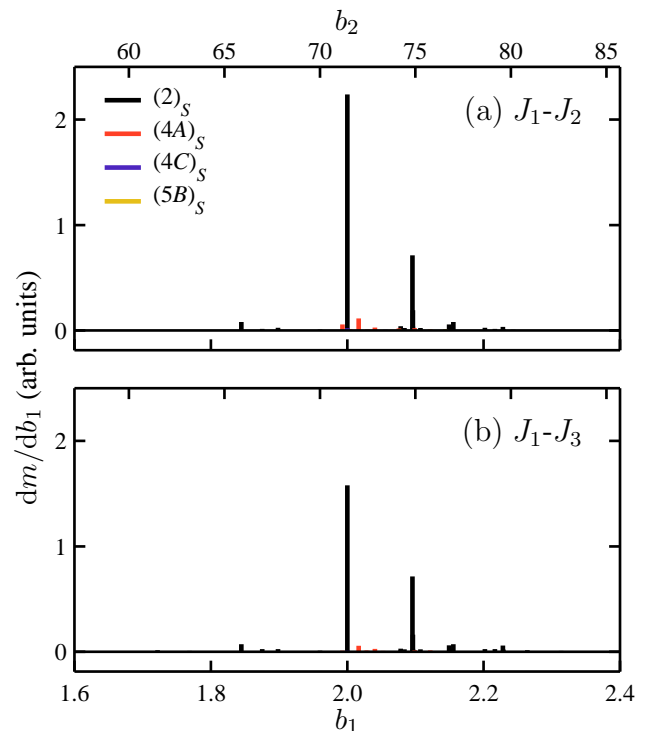


FIG. 10: (a) The full spectrum of the J_1 - J_2 model near $b_1=2$, calculated for $x=0.16$, $J_2/J_1=0.028$, $S=5/2$, and $T=0$. Only lines belonging to the $(2)_S$, $(4A)_S$, $(4C)_S$ and $(5B)_S$ mono-skeleton spectra are in this field range. The $(4C)_S$ and $(5B)_S$ lines are invisible in this figure because their intensities are very low. (b) The analogous results for the J_1 - J_3 model. The lower and upper abscissa scales are for the primary and secondary reduced field, b_1 and b_2 , respectively.

model also has a line at $b_1=2$, so that the $(4C)_S$ mono-skeleton FS will also contribute to this poly-skeleton FS. Finally, cluster type $5B$ of the J_1 model has a line at $b_1=2.166$, which is not too far from 2. Depending on the ratio J_2/J_1 , the $(5B)_S$ mono-skeleton FS may also contribute to the poly-skeleton FS near $b_1=2$.

Figure 10(a) shows the full spectrum of the J_1 - J_2 model near $b_1=2$, calculated for $x=0.16$ with $J_2/J_1=0.028$. Only strong lines are visible in this figure. The weak lines are seen clearly in Fig. 11(a) which uses a log scale for the line intensities. As expected, the poly-skeleton spectrum in this field range is composed of four mono-skeleton FS's: $(2)_S$, $(4A)_S$, $(4C)_S$, and $(5B)_S$. The relative intensities of spectral lines are always governed by cluster statistics. In Figs. 10(a) and 11(a) the strongest lines are from the $(2)_S$ mono-skeleton FS. As discussed later, the two most intense lines in this portion of the spectrum are very useful for an experimental determination of $J^{(2)}$.

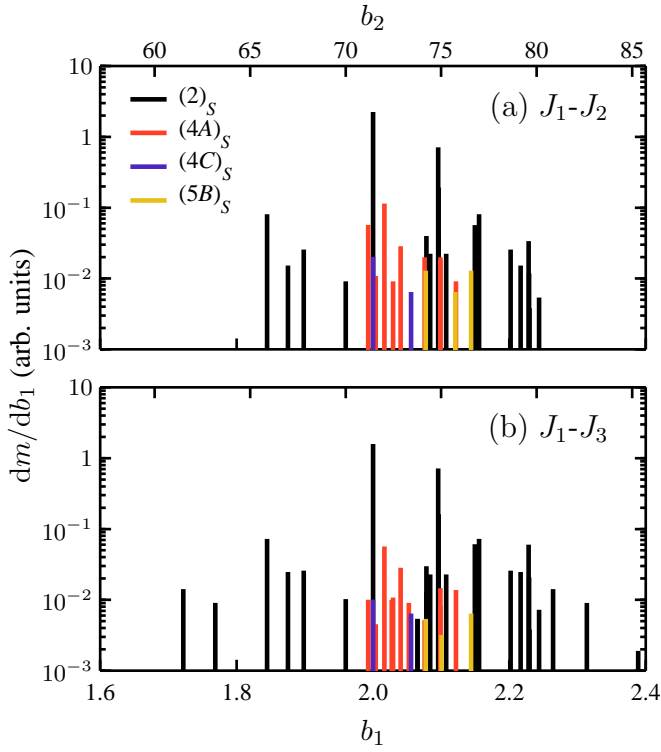


FIG. 11: The spectra in Figs. 10(a) and 10(b), replotted using a log scale for the line intensities.

D. Physical interpretation

1. Changes of exchange and Zeeman energies at MST's

Consider any cluster type other than a single. A MST, and the associated spectral line, occur at a magnetic fields B where a crossing of two energy levels changes the ground state. The energy E is the sum of the exchange energy E_{ex} and Zeeman energy E_Z . At any MST the difference ΔE_{ex} between the exchange energies of the two levels that cross is equal and opposite to the difference ΔE_Z between their Zeeman energies.

At any MST, the z component (along \mathbf{B}) of the ground-state total spin changes by one. For the energy levels that cross, ΔE_Z is therefore proportional to B , and so is ΔE_{ex} . Thus, at any high-field spectral line (above the gap) the changes ΔE_Z and ΔE_{ex} are larger than at any low-field line. The reduced fields b_1 at the high-field lines are of order 1 or larger. The change $|\Delta E_Z| = |\Delta E_{\text{ex}}|$ at any high-field line is therefore of order $|J_1|$ or larger.

2. Physical interpretation of a mono-skeleton fine structure

The exchange energy of a cluster is due to all the exchange bonds. Each bond is between two spins. The abrupt change ΔE_{ex} at any MST is caused by an abrupt change in the relative orientations of spins that are on

opposite sides of one, or more, exchange bonds. To produce a change ΔE_{ex} of order $|J_1|$, or larger, at any of the high-field lines, one or more of these bonds must be a J_1 bond. The small number of J_2 bonds in any of the clusters in Figs. 1 and 2 cannot produce a sufficiently large ΔE_{ex} when the ratio J_2/J_1 is so small that there is a gap in the spectrum. All the J_1 bonds are in the skeleton. Therefore, at any high-field line there is an abrupt change in the relative orientations of skeleton-spins.

All skeleton-spins are attached to J_1 bonds. However, some skeleton-spins may also be attached to J_2 bonds. At some high-field lines, simultaneous abrupt changes in the energies of both J_1 bonds and J_2 bonds may occur. However, the major contribution to ΔE_{ex} is from one or more of the strong J_1 bonds.

The arrangement of the strong J_1 bonds in a simple skeleton is fully specified by the skeleton type. The arrangement of the J_1 bonds in a fragment of the same type is identical. Therefore one expects that spectral lines produced by all simple skeletons and fragments of one type will involve nearly equal changes in the energy of the J_1 bonds. Because the energy change from the J_1 bonds is the major contribution to ΔE_{ex} , and because the magnetic field B at the MST is proportional to ΔE_{ex} , all lines from skeletons and fragments of the same type should occur at approximately the same field B . The small differences, ΔB , are due to differences in the minor contribution to ΔE_{ex} from the J_2 bonds. Different cluster types with the same skeleton/fragment type have different decorations, with different arrangements of J_2 bonds. It is these different decorations that are responsible for the small line separations, $\Delta b_2 \sim 1$, in the mono-skeleton FS.

V. LOW-FIELD SPECTRA

A. General conclusions from numerical simulations

MST's in the low-field part of the spectrum involve only the weak exchange bonds, i.e., J_2 or J_3 bonds. The strong J_1 bonds are not involved. Spins coupled by weak bonds occur in pure- J_2 or pure- J_3 cluster types, and in mixed cluster types. The low-field lines from pure- J_2 and pure- J_3 cluster types have already been discussed in Sec. II B. The remaining discussion therefore focuses on the mixed cluster types. A mixed cluster always has both a skeleton and a decoration. The decoration is either spinned or spinless.

Numerically-simulated spectra from many cluster types of the lopsided J_1 - J_2 model have already been presented in Figs. 5–9. The panels on the right of the lower parts of Figs. 5, 6, and 8(a) show the low-field spectra from all mixed cluster types of this model that have sizes $n_c \leq 5$. These low-field spectra lead to the following general conclusions:

1. Some cluster types with spinned decorations produce low-field lines, but others do not. The cluster

types that do, and those that do not, will be listed in Sec. VB. The physics behind these lists will be discussed in the same section.

2. Cluster types with spinless decorations do not produce low-field lines if the cluster size is $n_c \leq 5$. Therefore, none of the spinless decorations in Figs. 1 and 2 produce low-field lines. However, it will be shown in Sec. VC that spinless decorations in some cluster types of sizes $n_c > 5$ can produce low-field lines.

The following discussion is for the lopsided J_1 - J_2 model. Analogous results apply to the lopsided J_1 - J_3 model.

B. Low-field MST's from spinned decorations of the lopsided J_1 - J_2 model

Any decoration-spin is attached to one or more J_2 bonds, but not to any J_1 bond. A J_2 bond which is attached to a decoration-spin must also be attached either to another decoration-spin or to a skeleton-spin. The two cases are considered separately.

1. J_2 bond between two decoration-spins

Any cluster type with a J_2 bond between two decoration-spins always produces one or more low-field spectral lines. Examples are the low-field lines of cluster types 4-10, 5-23, 5-26, 5-27, 5-29, and 5-31 up to 5-35. With the exception of cluster type 5-27, which will be discussed separately, the relevant J_2 bond is not frustrated. That is, the two decoration-spins attached to the J_2 bond are antiparallel at $B=0$. Low-field MST's, in reduced fields b_2 of order 1, correspond to a stepwise alignment of these decoration-spins. At the completion of these low-field MST's, the decoration-spins attached to the J_2 bond are parallel.

The preceding argument does not apply to cluster type 5-27. The three J_2 bonds that are connected to the two decoration-spins cannot be all satisfied at $B=0$. The strong J_1 bonds lead to a parallel alignment of the two end-spins in the skeleton. To satisfy the J_2 bonds between these two end-spins and the two decoration-spins, the two decoration-spins must be parallel to each other. But then the J_2 bond between the two decoration-spins will not be satisfied. Thus, frustration of at least one of these three J_2 bonds is inevitable. Because of this frustration, the spin configuration in the zero-field ground-state of cluster type 5-27 is not immediately obvious.

The following physical picture for cluster type 5-27 is based, in part, on the results in Fig. 6. In the zero-field ground state the net spin of the skeleton alone is $S_S(0)=5/2$; the two parallel end-spins of the skeleton are antiparallel to the middle spin. The two decoration-spins, in this zero-field ground state, have a net spin $S_D(0)=2$. The two J_2 bonds between the skeleton's end-spins and

the decoration-spins cause the net spin of the decoration to be antiparallel to net spin of the skeleton. The zero-field ground state of the entire cluster therefore has a total spin $S_c(0)=5/2-2=1/2$.

Cluster type 5-27 has seven MST's in low fields. At each of these MST's the total spin S_c of the cluster's ground state increases by one unit. At the completion of these seven MST's, the decoration-spins and the end-spins of the skeleton are all parallel to each other. The decoration spin then has a magnitude $S_D=5$, and it is parallel to the skeleton's net spin whose magnitude is still $S_S=5/2$. Thus, at the completion of the seven low-field MST's, $S_c=15/2$ for the entire cluster. Five MST's above the gap in the spectrum, increase S_S from $5/2$ to $15/2$, with no change in S_D which remains saturated at 5. All spins of the cluster are then parallel, so that $S_c=25/2$.

2. J_2 bonds between decoration-spins and skeleton-spins

The only spinned decorations that are not covered by the preceding discussion are those in which all J_2 bonds that are attached to decoration-spins are also attached to skeleton-spins. Among the many cluster types with such spinned decorations, some produce low-field lines but others do not. The number of low-field lines (zero if there are no low-field lines) can be obtained as follows.

The total spin S_c of the cluster's ground state changes by unity at each MST. Therefore, the total number of MST's, N^{TOT} , for a cluster type c with size n_c is given by

$$N^{\text{TOT}} = n_c S - S_c(0), \quad (4)$$

where $n_c S$ and $S_c(0)$ are the saturation and zero-field values of S_c , respectively. Similarly, the number of MST's in the high-field region, N^{HF} , is

$$N^{\text{HF}} = n_S S - S_S(0), \quad (5)$$

where $n_S S$ and $S_S(0)$ are the saturation value and the zero-field value of the skeleton's ground-state spin, respectively. The number N^{LF} of low-field MST's is

$$N^{\text{LF}} = N^{\text{TOT}} - N^{\text{HF}}. \quad (6)$$

For the cluster types under consideration, $S_S(0)$ and $S_c(0)$, can be obtained by inspection because in the zero-field ground state none of the J_1 bonds (all in the skeleton) are frustrated, and none of those J_2 bonds that are between skeleton-spins and decoration-spins are frustrated. Using $S_S(0)$ and $S_c(0)$, Eqs. (4)–(6) then give N^{TOT} , N^{HF} , and N^{LF} . Table I gives the results for all the relevant cluster types, assuming that $S=5/2$. All the values of N^{LF} in this table agree with the simulations [see the low-field results in Figs. 5, 6, and 8(a)].

TABLE I: Properties of those cluster types of the lopsided J_1 - J_2 model for which all J_2 bonds that are attached to decoration-spins are also attached to skeleton-spins. It is assumed that $S=5/2$. N^{TOT} is the total number of MST's. N^{HF} is the number of high-field MST's (above the gap), and N^{LF} is the number of low-field MST's. The saturation value of the cluster's spin is $n_c S$. For the skeleton alone, the saturation value is $n_S S$. In the zero-field ground state, the cluster's spin is $S_c(0)$, and the skeleton's spin is $S_S(0)$.

Cluster Type	$n_c S$	$S_c(0)$	N^{TOT}	$n_S S$	$S_S(0)$	N^{HF}	N^{LF}
3-3	15/2	5/2	5	5	0	5	0
4-6	10	0	10	15/2	5/2	5	5
4-7	10	0	10	15/2	5/2	5	5
4-8	10	5	5	15/2	5/2	5	0
4-9	10	0	10	5	0	5	5
4-11	10	5	5	5	0	5	0
5-12	25/2	5/2	10	10	0	10	0
5-13	25/2	5/2	10	10	0	10	0
5-14	25/2	5/2	10	10	0	10	0
5-15	25/2	5/2	10	10	0	10	0
5-16	25/2	5/2	10	10	0	10	0
5-17	25/2	5/2	10	10	0	10	0
5-18	25/2	5/2	10	10	5	5	5
5-19	25/2	5/2	10	10	5	5	5
5-20	25/2	5/2	10	10	0	10	0
5-21	25/2	5/2	10	15/2	5/2	5	5
5-22	25/2	5/2	10	15/2	5/2	5	5
5-24	25/2	5/2	10	15/2	5/2	5	5
5-25	25/2	5/2	10	15/2	5/2	5	5
5-28	25/2	5/2	10	15/2	5/2	5	5
5-30	25/2	5/2	10	10	0	5	5
5-39	25/2	5/2	10	10	0	10	0
5-40	25/2	5/2	10	10	0	10	0
5-41	25/2	5/2	10	10	0	10	0

C. Physical picture for the absence or presence of low-field MST's from spinless decorations

When the decoration is spinless, all spins of the cluster are skeleton-spins. The skeleton is either simple or compound. The two cases are considered separately.

1. Simple skeletons

A cluster with a simple skeleton and a spinless decoration does not produce low-field lines. The reasons are as follows. Any two spins in the cluster are connected by a continuous path (or paths) of J_1 bonds. For the cluster sizes considered here, any such a " J_1 bridging path" is relatively short, i.e., the number of J_1 bonds in the path is of order 1. An energy of order $|J_1|$ is required to produce an abrupt change of the relative orientations of spins in such a bridging path.

Because the decoration is spinless, any weak bond (J_2 bond) is between two skeleton-spins. These two skeleton-spins are also connected by one or more J_1 bridging

paths. (For examples see cluster types 4-2 up to 4-5, and 5-2 up to 5-11, in Figs. 1 and 2). If a low-field MST occurs, it must arise from abrupt changes in the relative orientations of skeleton-spins that are coupled by J_2 bonds. But such abrupt changes will always be accompanied by an abrupt energy change of order J_1 from at least one J_1 bridging path. An energy change of order J_1 is incompatible with the assumption that the MST is in the low-field part of the spectrum.

2. Compound skeletons

The preceding arguments for a spinless decoration may fail if the skeleton is compound rather than simple. The reason is that at least one J_2 bond is between spins in different fragments. Such spins are not connected by a J_1 bridging path.

In the zero-field ground state of the cluster, each fragment has a net spin, say, \mathbf{S}_{F1} for one fragment and \mathbf{S}_{F2} for the other. If neither of these fragment-spins is zero at $B=0$ then the J_2 bond(s) between the fragments will cause \mathbf{S}_{F1} and \mathbf{S}_{F2} to be antiparallel in zero field. In the low-field region (b_2 of order 1), a series of MST's will then take place. This low-field series will end when \mathbf{S}_{F1} and \mathbf{S}_{F2} become parallel.

As an example, consider a cluster type of size $n_c=6$ with a $(3)_S$ - $(3)_S$ compound skeleton. The two $(3)_S$ fragments are coupled by only one J_2 bond. The spinless decoration consists of the lone J_2 bond linking the fragments. The spin arrangement in the zero-field ground state is represented by $(+++) \cdots (---)$, where the dotted line is the J_2 bond between the fragments. Each fragment then has a spin $S_F=5/2$. The antiferromagnetic J_2 bond leads to a zero net spin for the entire cluster. Five MST's will occur in low-fields, ending with the spin arrangement $(+++) \cdots (---)$. The cluster's net spin is then 5. Additional MST's that involve the J_1 bonds within the fragments will occur in the high-field region.

The preceding example involved a cluster type of size $n_c>5$. When $n_c \leq 5$, at least one fragment of the compound skeleton is a $(2)_S$ fragment. In the zero-field ground state, this fragment has net spin $S_{F1}=0$. The $(2)_S$ fragment is therefore not responsive to a magnetic field in low fields. The fragment becomes responsive only when S_{F1} can change from zero. The first such possibility is when b_1 is near 2, where S_{F1} can change from zero to 1. Regardless of whether the other fragment is of type $(2)_S$ or of type $(3)_S$, there are no MST's in the low-field part of the spectrum, which is well below $b_1=2$.

In summary, in order for a spinless decoration to produce MST's in the low-field part of the spectrum, it is necessary that: 1) the skeleton is compound, and 2) the cluster size is $n_c>5$. These necessary conditions are not always sufficient.

VI. MEASUREMENT OF THE SECOND-LARGEST EXCHANGE CONSTANT

It is assumed that the second-largest exchange constant $J^{(2)}$ is either J_2 or J_3 . Two issues of interest to experimentalists are: 1) What features of a measured spectrum are most useful for determining the magnitude of $J^{(2)}$? 2) Is there a practical way of deciding whether $J^{(2)}$ is J_2 or J_3 ?

A. Determination of $J^{(2)}$ from the low-field spectrum

For both the J_1 - J_2 and J_1 - J_3 models, cluster type 2-2 corresponds to a pair in which the two spins are coupled by $J^{(2)}$. When the models are lopsided, these 2-2 pairs produce the strongest lines in the low-field part of the spectrum, at least up to $x=0.20$ (see Fig. 13 of II). The magnetic fields at these strongest low-field lines yield $J^{(2)}$ via Eqs. (3b) and (6b) of II.

To resolve the 2-2 lines, the line width δB must be smaller than the field separation between adjacent lines, $\Delta B=2|J^{(2)}|/g\mu_B$, or $\Delta b_2=2$. Thermal broadening, proportional to T , places a lower limit on the line width δB (see, e.g., Ref. 4). For a lopsided model, $J^{(2)}$ can be so small that very low temperatures are required to resolve the 2-2 lines.

B. Determination of $J^{(2)}$ from high-field FS

The high-field FS near $b_1=2, 4, \dots, 10$ provides an alternative route for determining $J^{(2)}$. Figures 10(a) and 10(b) illustrate the FS near $b_1=2$ in the J_1 - J_2 and J_1 - J_3 models, respectively. In both models the 2-1 line, from J_1 pairs, is the strongest. The second-strongest line is from 3-3 triplets, each of which consists of a J_1 pair attached to a third spin by a $J^{(2)}$ bond. Both the 2-1 and the 3-3 lines belong to the $(2)_S$ mono-skeleton FS.

The 2-1 and 3-3 lines are the strongest two lines not only in the FS near $b_1=2$, but also in the FS near each of the values $b_1=2n$, where $n=1, 2, \dots, 5$. (The groups of very close lines near $b_1=2, 4$, and 6 are shown in Fig. 12 of Ref. 2.) The separation ΔB between the 2-1 and 3-3 lines was calculated earlier for all values of n .^{4,5} The results, as a function of $J^{(2)}/J^{(1)}$, are reproduced in Fig. 12. The ordinate is the field separation in reduced units, $\Delta b_2 = g\mu_B \Delta B / |J^{(2)}|$. Figure 12 indicates that Δb_2 is largest for $n=1$, i.e., near the first MST from pure J_1 pairs. The measured separation between the 2-1 and 3-3 lines close to $b_1=2$, together with the results in Fig. 12, can be used to determine $J^{(2)}$.

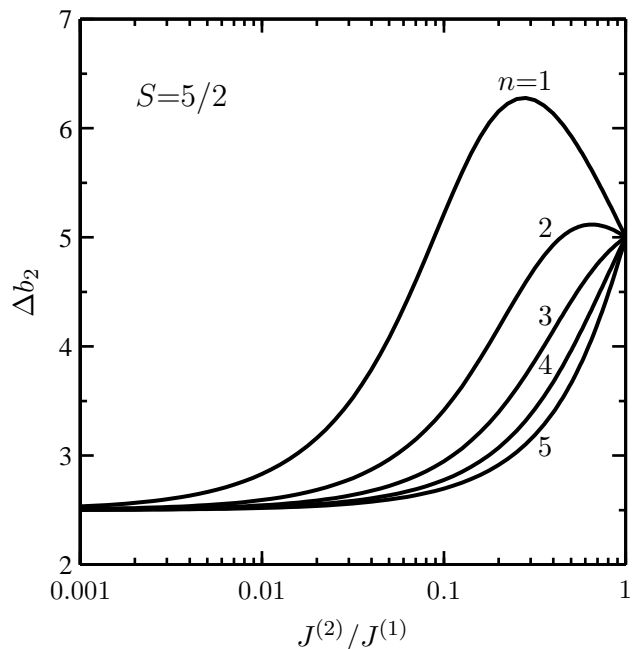


FIG. 12: The separation Δb_2 between the secondary reduced fields b_2 at the 3-3 and 2-1 lines that are near $b_1=2n$. These results, for $n=1, 2, \dots, 5$, are plotted as a function of $J^{(2)}/J^{(1)}$. The curves for $J^{(2)}/J^{(1)} \leq 1$ apply to both the lopsided J_1 - J_2 and the lopsided J_1 - J_3 models. (Adapted from Refs. 4 and 5).

C. Difficulty of identifying $J^{(2)}$ as J_2 or J_3

The spectra and magnetization curves obtained from the J_1 - J_2 and J_1 - J_3 models are not identical. In principle, it should be possible to distinguish between J_2 or J_3 by comparing the measured spectrum and/or magnetization curve with simulations based on the two models.^{3,4,6} Because the simulations assume a random distribution of the magnetic ions over the cation sites, conclusions concerning the identity of $J^{(2)}$ that are based on such comparisons hinge on this assumption. A random distribution has been found in many materials, but deviations (sometimes large) have also been observed (see Ref. 4).

In practice, even if the distribution is random it may be difficult to distinguish between J_2 and J_3 . The basic reason is that the number of 2nd and 3rd neighbors is the same, namely, 4. Although spectra calculated from the J_1 - J_2 and J_1 - J_3 models are not identical, the differences are often quite subtle. Many of these differences are in the low-intensity lines (compare, for example, the two parts of Fig. 11). Obviously, these are just the lines that are the most difficult to observe and measure accurately.

The comparison of the magnetization curve, rather than the spectrum, with simulations may be more promising. The change of M in a field interval that includes many spectral lines is the sum of the integrated intensities of these lines. Small differences between many weak spectral lines in the two models result in somewhat

different magnetization curves when x is not very small.

Acknowledgments

This work was supported by CNPQ and FAPESP. Travel funds for Y. S. were also provided by FAPESP.

APPENDIX A: THE CORRECTIVE QUINTETS METHOD

The CQUIN's method for the J_1 model was described in I. For a cluster model with two AF exchange constants the CQUIN's method involves many more steps, and is much more elaborate. The method is appropriate when the two exchange constants have very different magnitudes. This is always the case when the model is lopsided.

1. Corrective and real quintets

The CQUIN's method is used only in the calculation of M , not in the calculation of dM/dB (see Sec. VI of Ref. 2). The infinite sum in Eq. (2) of Ref. 2 cannot be carried out. Therefore, it is truncated after a finite number of terms. When the CQUIN's method is used, the truncated sum includes only clusters of sizes $n_c \leq 5$. The CQUIN's method replaces the remainder by an ensemble of fictitious clusters of size $n_c = 5$. These fictitious quintets are the corrective quintets (CQUIN's).

The ensemble of CQUIN's is specified by giving the cluster types of the CQUIN's, and the cluster population for each type. The description below is for the J_1 - J_2 model, assuming that the ratio J_2/J_1 is small. The CQUIN's method for the J_1 - J_3 model is similar.

It is important to distinguish between “real quintets” and CQUIN's. The real quintets are included in the finite truncated sum of Eq. (2) of Ref. 2 (hereafter called the “truncated sum”). The CQUIN's are fictitious quintets whose only purpose is to approximate the remainder. The cluster types of the CQUIN's are the same as the cluster types of the real quintets, i.e., they are all the quintet types of the J_1 - J_2 model. The remaining task is to specify the population (number of CQUIN's) for each of these types.

2. Guidelines for selecting the populations of CQUIN's

Two guidelines, or principles, are used to specify the populations of the various types of CQUIN's. First, the ensemble of CQUIN's should include a collection of skeletons which resembles, to the extent possible, the collection of skeletons in the remainder. The rationale is that the MST's in the high-field part of the spectrum are

largely controlled by the skeletons. An inherent limitation is that skeletons of CQUIN's are all of sizes $n_S \leq 5$, whereas some skeletons in the remainder have larger sizes. The CQUIN's can only approximate the magnetization from the remainder, they cannot reproduce it exactly.

The second guideline demands that after all the CQUIN's are included, the calculated magnetization M in the limit $B \rightarrow \infty$ will have the true saturation value. This means that the total number of spins in the ensemble of CQUIN's must equal the total number of spins in the remainder. This number is $P_{>5}N_{\text{total}}$.

3. Role of the parent J_1 model

The parent J_1 model plays a major role in the CQUIN's method. One reason is that the definitions of a simple-skeleton type, and of a fragment type, are based on a comparable cluster type c in the parent J_1 model. The comparable cluster type has the same set of J_1 bonds. The “single” is the only cluster type c of the J_1 model that has no corresponding skeleton/fragment type $(c)_S$.

Consider one realization of any cluster type c of the parent J_1 model, except a single. When the J_1 model is replaced by the J_1 - J_2 model, the spins that were earlier in this realization form a simple skeleton, or a fragment, of type $(c)_S$. These skeletons and fragments will be incorporated into many cluster types of the J_1 - J_2 model.

The skeletons/fragments of type $(c)_S$ that are incorporated into clusters of sizes not exceeding 5 are in the truncated sum. These skeletons and fragments will be treated exactly. The other skeletons/fragments of type $(c)_S$ are incorporated into clusters larger than quintets, which are in the remainder. The simple skeletons and fragments of type $(c)_S$ that are in the remainder will be represented by those in the CQUIN's.

If possible, the collection of CQUIN's should contain the total number of skeletons/fragments of type $(c)_S$ that are in the remainder. The limitation is that CQUIN's contain only simple skeletons of sizes $n_S \leq 5$, and only fragments of sizes $n_F = 2$ or 3. Those skeletons and fragments in the remainder which conform to these size limitations can be well represented by CQUIN's. Larger skeletons and fragments in the remainder cannot be well represented by CQUIN's.

In view of the limitation just mentioned, the only cluster types c of the J_1 model that are considered explicitly are those with sizes up to 5. The population N_{c0} , in the J_1 model, of each of these cluster types c is counted at the start of the CQUIN's method. This count is called the “initial count” for type c .

Cluster types c of the J_1 model that have sizes $n_c > 5$ are not treated explicitly. However, these cluster types are not totally ignored. An allowance for J_1 -clusters larger than quintets is made by increasing the initial counts N_{c0} for all the quintet types c of the J_1 model by ΔN_{c0} . These ΔN_{c0} are obtained from the CQUIN's procedure

for the J_1 model.¹ The adjustments ΔN_{c0} are carried out only for the quintet types of the J_1 model, not for other cluster types.

4. Adding CQUIN's in stages

The ensemble of CQUIN's that replaces the remainder is assembled in stages. At each stage CQUIN's with skeletons and fragments of only one type, $(c)_S$, are added. The sequence of stages is discussed later. The following is a description of any one of these stages.

At the beginning of a stage, all skeletons and fragments of type $(c)_S$ that have already been included in the calculation of M are counted. This count is called the "second count" for type c . The result of the second count will be called N_c^* . In most cases N_c^* includes only the skeletons and fragments of type $(c)_S$ that are in the truncated sum. The only exception is in the second count of skeletons/fragments of type $(2)_S$, performed at the beginning of the stage in which CQUIN's with $(2)_S$ skeletons/fragments are added. As explained below, CQUIN's with $(3)_S$ fragments are added in an earlier stage which is devoted to $(3)_S$ skeletons and fragments. What complicates matters is that whenever a $(3)_S$ fragment was added, a $(2)_S$ fragment was automatically added at the same time. The reason is that a skeleton of a CQUIN with a $(3)_S$ fragment is always of type $(3)_S$ - $(2)_S$. The $(2)_S$ fragments that were introduced before the beginning of the stage devoted to $(2)_S$ skeletons/fragments must be included in the second count for this stage.

The CQUIN's types that are added at any one stage include all the quintet types of the J_1 - J_2 model that have skeletons and fragments of type $(c)_S$. The populations of these CQUIN's types are determined by two rules: 1) The total number of skeletons and fragments of type $(c)_S$, in all the CQUIN's that are added at this stage, is equal to the difference $(N_{c0} - N_c^*)$ between the initial and second counts for type c . This requirement fulfills the first guideline in part A 2 of this Appendix. 2) The ratios between populations of different CQUIN's types that are added in any stage must be equal to the population ratios for real quintets of the same types.

5. Order of the various stages of the CQUIN's method

Each stage of adding CQUIN's is related to a particular cluster type c of the J_1 model. The sequence of stages follows the order of decreasing cluster size n_c , in the J_1 model. The 10 cluster types of the J_1 model lead to 10 stages.

Stages 1-4

The first four stages treat the four quintet types of the J_1 model: $5A$, $5B$, $5C$, and $5D$. The order of these four stages is arbitrary. Consider quintet type $5A$. Figure 2 shows that the second count will only include the $(5A)_S$ skeletons in real quintets of types 5-1 up to 5-6. The CQUIN's types that are added in this stage are also 5-1 up to 5-6.

Cluster types $5B$, $5C$, and $5D$, of the J_1 model are handled in a similar way, in three separate stages. For $5C$, the second count involves only the $(5C)_S$ skeletons of real quintets of type 5-10. The CQUIN's that are added in this stage are also of type 5-10. A similar remark applies to the stage devoted to cluster type $5D$ of the J_1 model.

Stages 5-7

These stages treat the three quartet types of the J_1 model: $4A$, $4B$, and $4C$. Again, the order is arbitrary. The second count for quartet type $4A$ includes the $(4A)_S$ skeletons in the quartet types 4-1, 4-2, and 4-3 (Fig. 1), and in real quintets of types 5-12 up to 5-17 (Fig. 2). The cluster types of the CQUIN's are 5-12 up to 5-17. Quartet types $4B$ and $4C$ of the J_1 model are handled in a similar way, in separate stages.

Stage 8

This stage treats the only triplet type (type 3) of the J_1 model. The second count includes the $(3)_S$ skeletons of the following cluster types: 3-1, 3-2, 4-6 up to 4-8, and real quintets of types 5-21 up to 5-29. The second count also includes the $(3)_S$ fragments in the $(3)_S$ - $(2)_S$ skeletons of real quintets of types 5-36 up to 5-38. The cluster types of the CQUIN's are 5-21 up to 5-29, and 5-36 up to 5-38. Note that CQUIN's of types 5-36 up to 5-38 contain $(2)_S$ fragments, in addition to $(3)_S$ fragments. Therefore, already at this stage some $(2)_S$ fragments are added to the ensemble of CQUIN's.

Stage 9

This stage involves the pairs (cluster type 2) of the J_1 model. The second count includes the $(2)_S$ skeletons of the cluster types 2-1, 3-3, 4-9 up to 4-11, and real quintets of types 5-30 up to 5-35. Also included are the $(2)_S$ fragments of the $(2)_S$ - $(2)_S$ skeletons in quartets of type 4-12, and in real quintets of types 5-39 up to 5-41. The $(2)_S$ fragments in $(3)_S$ - $(2)_S$ skeletons of real quintets of types 5-36 up to 5-38 are also included in the second count. Finally, the $(2)_S$ fragments in the CQUIN's of types 5-36 up to 5-38, which were added in stage No. 8,

are included. The CQUIN's that are added in stage 9 are of types 5-30 up to 5-35, and 5-39 up to 5-41.

Final Stage: CQUIN's that are pure J_2 clusters

The final (10th) stage corrects for the “missing singles” of the J_1 model. The single is the only cluster type of the J_1 model which has no corresponding skeleton type, or fragment type. Therefore, the CQUIN's that are added in the final stage have no skeletons; they are pure J_2 clusters.

The initial count N_{10} is the number of singles in the J_1 model. When the J_1 model is replaced by the J_1 - J_2 model, the former singles end up in cluster types of the J_1 - J_2 model. Some remain as singles (cluster type 1-1 in the new J_1 - J_2 model). Some others end up in pure J_2 clusters, and the rest end up in spinned decorations of mixed J_1 - J_2 clusters.

The former singles of the J_1 model that end up in clusters of sizes up to 5 are in the truncated sum. These spins are included in the second count N_1^* . The second count also includes the spins in all spinned decorations of the CQUIN's that were introduced in the earlier stages. The CQUIN's types that are added in the final (10th) stage are the pure- J_2 quintet types of the J_1 - J_2 model, namely, cluster types 5-42 up to 5-45 in Fig. 2. The total number of spins in these newly added CQUIN's is $(N_{10}-N_1^*)$.

6. Example

An example of the application of the CQUIN's method is shown in Fig. 13. The various curves represent the reduced magnetization m , in the J_1 - J_2 model, after the completion of various stages in the CQUIN's procedure. The curve labeled as “0” represents the truncated sum alone, without any CQUIN's. The curve labeled as “4” is the calculated magnetization after the completion of stages 1–4. The curves labeled as “7”, “8”, “9”, and “10”, represent the magnetization after the completion of stages 5–7, 8, 9, and 10, respectively. The curve labeled as 10 is the final result.

The dashed curve between the curves “0” and “4” has the following meaning. Each of the initial counts N_{c0} for quintets of types c of the J_1 model contains two contributions (see section A 3 of this appendix). The first is the actual initial population count for quintets of this type. The second is the adjustment ΔN_{c0} , introduced to correct for neglecting clusters of the J_1 model that are

larger than quintets.

Each of the stages from 1 to 4 corrects for the difference $(N_{c0}-N_c^*)$ between the initial and second counts for one quintet type c . There are two contributions to this difference, corresponding to the two contributions to N_{c0} . The dashed curve in Fig. 13 represents the magnetization that would have been present at the completion of stages 1–4 if the only contribution to N_{c0} had been from the adjustment ΔN_{c0} .

Physically, the difference between the dashed curve and the curve “0” approximates the magnetization from those clusters in the remainder that contain simple skeletons or fragments of sizes larger than 5. The difference between the curve labeled as “4” and the dashed curve approximates the magnetization from those clusters in the remainder that have simple skeletons or fragments with 5 spins.

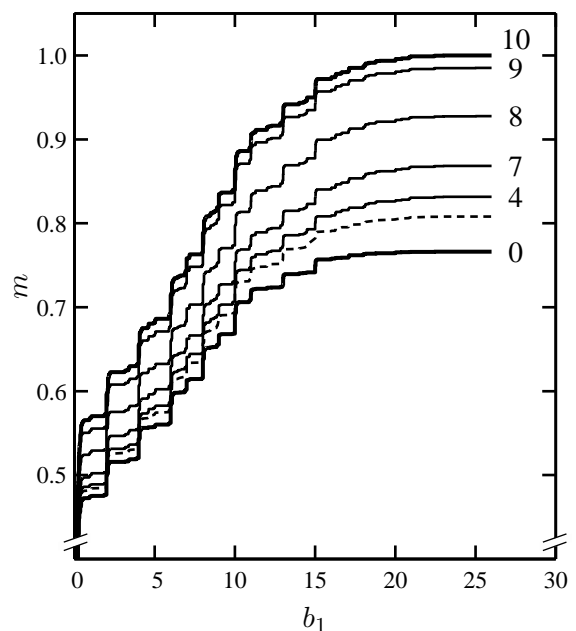


FIG. 13: An example of the CQUIN's method, showing the calculated magnetization after the completion of various stages. The example is for the J_1 - J_2 model, with $x=0.16$, $J_2/J_1=0.028$, $S=5/2$, and $T=0$. The abscissa is the primary reduced field b_1 . The ordinate is the reduced magnetization $m=M/M_0$. The curve labeled as “0” represents the truncated sum alone, before any CQUIN's are introduced. The curve labeled as “10” is the total magnetization, after all 10 stages of the CQUIN's method have been completed. The curves labeled as “4”, “7”, “8”, and “9”, represent the completion of the 4th, 7th, 8th, and 9th stages, respectively. The dashed curve is discussed in the text.

* Electronic address: yshapira@granite.tufts.edu

† Electronic address: vbindilatti@if.usp.br

¹ V. Bindilatti and Y. Shapira, Phys. Rev.

B **72**, 064414 (2005), also called I, URL <http://link.aps.org/abstract/PRB/v72/e064414>.

² Y. Shapira and V. Bindilatti, arXiv:cond-mat/0609715

- (2006), also called II; <http://arxiv.org/abs/cond-mat/0609715>.
- ³ X. Gratens, A. Paduan-Filho, V. Bindilatti, N. F. Oliveira, Jr., and Y. Shapira, to be published (2006).
- ⁴ Y. Shapira and V. Bindilatti, J. Appl. Phys. **92**, 4155 (2002), URL <http://link.aip.org/link/?jap/92/4155>.
- ⁵ T. Q. Vu, Ph.D. thesis, Tufts University (1992).
- ⁶ V. Bindilatti, E. ter Haar, N. F. Oliveira, Jr., Y. Shapira, and M. T. Liu, Phys. Rev. Lett. **80**, 5425 (1998), URL <http://publish.aps.org/abstract/PRL/v80/p5425>.